Solution Structure of the *Rhodobacter sphaeroides* PufX Membrane Protein: Implications for the Quinone Exchange and Protein−Protein Interactions[†,‡]

Zheng-Yu Wang,*[,§] Hiroaki Suzuki,[§] Masayuki Kobayashi,[||] and Tsunenori Nozawa[⊥]

Faculty of Science, Ibaraki University, Mito 310-8512, Japan, Ariake National College of Technology, Omuta, Fukuoka 836-8585, Japan, and National Institution for Academic Degree and University Evaluation, 1-29-1 Gakuen-nishimachi Kodaira-shi, Tokyo 187-8587, Japan

Received August 30, 2006; Revised Manuscript Received November 30, 2006

ABSTRACT: PufX membrane protein is found in *Rhodobacter* species of purple photosynthetic bacteria and has been known to play an essential role in ubiquinone/ubiquinol exchange between the reaction center and cytochrome bc_1 complex and also contribute to the dimerization of the reaction center−light-harvesting core complex. We have determined the solution structure of the *Rhodobacter sphaeroides* PufX using multidimensional NMR spectroscopy. The PufX, functionally expressed in *Escherichia coli*, forms a stable α helix consisting of 21 residues over the central transmembrane domain. The overall structure of the PufX is very similar to those of the LH1 α- and *β*-polypeptides from *Rhodospirillum rubrum* and LH2 polypeptides. A short segment (Lys28−Gly35) rich in Gly and Ala residues revealed a relatively fast exchange between the backbone amide protons and deuteriums in the hydroxyl groups of the solvent, indicating that the backbone of this segment is more easily accessible to the surrounding solvent molecules compared to those of its neighboring portions. The Gly- and Ala-rich segment is located in the middle of the central helix and forms an extensive groove-like conformation on the surface with the neighboring residues, where the residues with large side chains are aligned on one side of the helix, and small residues are aligned on the other face. Such a structural motif may serve as a functional site responsible for ubiquinol transport from the core complex to the membrane phase and for sequence-specific helix−helix interactions with the neighboring polypeptides.

Rhodobacter (*Rb.*[1]) *sphaeroides* is the most well-characterized photosynthetic bacterium and has been used as a model for studying the mechanism of photosynthesis. It can grow in a variety of conditions ranging from photoautotrophic growth, in the absence of oxygen using carbon dioxide as the sole carbon source, to chemoheterotrophic growth in the dark in the presence of oxygen using organic compounds as both a source of carbon and reducing power. For this reason, this bacterium has been subjected to a wide range of investigations from spectroscopy to biochemical manipulation, including site-directed mutagenesis. Like most other purple photosynthetic bacteria, *Rb. sphaeroides* collects solar energy by two types of light-harvesting complexes (LH1, LH2) and transfers it to the reaction center (RC) for primary charge separation. The LH1 complex exists in all purple bacteria and is located intimately around the RC with a fixed stoichiometric ratio, whereas the LH2 complex is arranged in the periphery of the LH1−RC complex with varied ratios to the RC and is lacking in some species such as *Rhodospirillum* (*R.*) *rubrum*. Both LH1 and LH2 are large oligomers of a basic structural unit composed of a heterodimer of two small integral membrane polypeptides (α and *β*, ca. 6 kDa) associated with bacteriochlorophyll (BChl) and carotenoid molecules. Although a number of high-resolution X-ray crystal structures have been determined for the RC (*1*−*3*) and LH2 (*4*, *5*), atomic information on the structure of LH1 complexes has not been established. Atomic force microscopy and 2D crystallographic studies show that the LH1 complex from *R. rubrum* forms a closed ring composed of 16 α*β* pairs around the RC (*6*−*8*). A similar structural feature was observed for the LH1−RC complex in the native photosynthetic membranes of *Rhodopseudomonas* (*Rps.*) *viridis* (*9*) and *R. photometricum* (*10*). However, a different structural organization has been reported for the LH1−RC complex of *Rb. sphaeroides*. Low-resolution electron microscope studies on the native membrane and crystals revealed a dimeric structure with an S-shaped arrangement of the LH1 α*β* subunit around the RC (*11*−*13*), where an additional protein, PufX, appears to be involved in the assembly of the core complex with a dimeric form. PufX, predicted as a membrane protein, has been postulated to be located near or at the dimer junction, but no precise structural information is available. The highest

[†] This work was supported by Grants-in-aid for Scientific Research on Priority Areas "Structures of Biological Macromolecular Assemblies", the Ministry of Education, Science, Sports and Culture, Japan.

[‡] Coordinates have been deposited in the Protein Data Bank (entry 2DW3).

* Corresponding author. Fax: +81-29-228-8352. E-mail: wang@mx.ibaraki.ac.jp.

[§] Ibaraki University.

[||] Ariake National College of Technology.

[⊥] National Institution for Academic Degree and University Evaluation.

[1] Abbreviations: BChl, bacteriochlorophyll; *E*, *Escherichia*; LH1, core light-harvesting; LH2, peripheral light-harvesting; RC, reaction center; *Rps*, *Rhodopseudomonas*; *R*, *Rhodospirillum*; *Rb*, *Rhodobacter*.

10.1021/bi0618060 CCC: $37.00
Published on Web 03/03/2007

resolution structure of LH1−RC complexes obtained so far was from *Rps. palustris* (*14*). It shows that the RC is surrounded by an oval LH1 complex consisting of 15 pairs of $\alpha\beta$ polypeptides, and the repeating $\alpha\beta$ units are interrupted by an unknown protein W. This protein has been proposed to be analogous to the PufX protein.

The PufX membrane protein in *Rhodobacter* species has been shown to play an essential role in promoting efficient light-driven electron transfer under anaerobic conditions (*15*, *16*) and in facilitating fast ubiquinone/ubiquinol exchange between the RC and cytochrome bc_1 complex (*17*). However, the expression of the PufX protein in the native membrane is very low, about 1 copy to 15 copies of LH1 α- or β-polypeptides. It is also difficult to purify the PufX protein from natural sources because of its hydrophobic nature (*18*). In a previous study (*19*), we reported the results on the expression of the *Rb. sphaeroides* PufX membrane protein using *Escherichia* (*E.*) *coli* cells. PufX was overexpressed as a recombinant protein with a histidine tag added to the carboxyl terminus and could be extracted from the cell membrane by various detergents. The PufX expressed was examined by reconstitution experiments with LH1 α- and β-polypeptides and BChl *a*. It was shown that PufX inhibited not only the reconstitution of the LH1 complex but also the formation of the B820 subunit type complex at high concentrations, indicating that the PufX expressed is biologically active. The large scale expression of the functional PufX membrane protein provides sufficient quantity for further determination of its 3D structure.

In this study, we present results on the solution structure of the *Rb. sphaeroides* PufX membrane protein expressed in *E. coli* using multidimensional NMR spectroscopy. A high-resolution structure is obtained in mixed organic solvents using ^{13}C- and ^{15}N-labeled samples. The PufX protein exhibits a long α helical region over the central transmembrane domain. The overall structural feature is very similar to those of the LH1 α- and β-polypeptides of *R. rubrum* (*20*). On the basis of the structural analysis, a possible functional segment of the PufX protein has been proposed.

MATERIALS AND METHODS

Sample Preparation. The *Rb. sphaeroides* PufX membrane protein was prepared as previously described (*19*). A 210 bp fragment of the *pufX* gene was cloned as a C-terminal His-tag fusion in pET20b(+) (Novagen) and expressed in *E. coli* strain BL21(DE3)pLysS. The PufX protein expressed was confirmed to be composed of 69 amino acids starting with a N-terminal Ala residue, followed by one leucine, one glutamic acid, and six histidine residues at the C-terminal end for a total of 77 residues. Uniformly isotope-labeled PufX proteins were prepared by growing the *E. coli* cells in the media developed in this laboratory (*21*). This involved the utilization of the hydrolysates of photosynthetic bacteria grown in isotopically labeled cultures. The ^{15}N- and ^{13}C/^{15}N-labeled PufX were obtained using the hydrolysates of *R. rubrum* and *Allochromatium vinosum* cells, respectively. For some experiments, commercial isotope cultures C. H. L. (Chlorella Industry Co., Ltd.) were also employed. After the induction of cell cultures with 1 mM isopropyl- β-D-thiogalactopyranoside for 12 h at 30 °C, the PufX protein was extracted by 0.5% (w/v) Triton X-100 and purified by a Ni-chelated IDA agarose resin column (His·Bind Resin, Novagen) and a reverse-phase HPLC column (TSKgel, ODS-80Ts, 21.5 mm × 300 mm, TOSOH) with a linear gradient (*19*).

NMR Spectroscopy. All NMR experiments were performed on a Bruker AVANCE DRX-400 spectrometer at 25 °C. A 5-mm TXI triple-resonance inverse probe with a *z*-axis field gradient was used. The PufX protein was directly dissolved in $CDCl_3/CD_3OH$ (1:1, v/v) at a concentration of 2 mM. Two-dimensional ^{1}H-^{15}N HSQC spectra were acquired with the pulse sequence of phase-sensitive echo/antiecho-TPPI gradient selection (*22*) using the ^{15}N-labeled samples. Sequential backbone assignments of ^{1}H, ^{13}C, and ^{15}N resonances were made using standard 3D triple-resonance HNCA (*23*), HN(CO)CA (*24*), CBCANH (*25*), CBCA(CO)NH (*26*), HBHANH (*27*), and HBHA(CO)NH (*28*) experiments. Side-chain resonances were assigned from 3D ^{15}N TOCSY-HSQC (*22*), H(CC)(CO)NH (*29*, *30*), CBCANH, and HBHANH data. The NOE-derived distance restraints were obtained from 3D ^{15}N NOESY-HSQC (*22*) spectra with a mixing time of 200 ms. The $^3J(H^N, H_\alpha)$ coupling constants were measured from the 3D HNHA spectrum (*31*) and were used to determine ϕ-angle restraints. Slow-exchanging amide protons were identified from a series of 2D ^{1}H-^{15}N HSQC spectra recorded over a 10 day period after dissolving the PufX protein in $CDCl_3/CD_3OD$ (1:1, v/v). Hydrogen-bonding strength was evaluated from the peak volume. Amide protons with half-lives longer than 48 h were classified as being hydrogen-bonded and those with half-lives longer than 96 h were classified as being strongly hydrogen-bonded. NMR spectra were processed with NMRPipe (*32*) and analyzed using NMRView (*33*).

Structure Calculations. Structures of the PufX protein were calculated by a distance geometry simulated annealing protocol using CNS (*34*). Distance restraints were obtained by converting NOE peak intensities into distance upper limits with d(strong) = 3.0 Å, d(medium) = 4.5 Å, and d(weak) = 5.5 Å. Each hydrogen bond was represented by two distance restraints (N−O, 2.4−3.0 Å and H^N−O, 1.9−2.3 Å) for maintaining linear bond geometry. The chemical shifts of $^{13}C_\alpha$ and $^{13}C_\beta$ were incorporated into the CNS calculation as additional torsion angle restraints (*35*). A total of 200 random structures were calculated and subjected to one cycle of 7000 steps of heating at 4000 K and 5000 steps of annealing followed by 1000 steps of conjugate gradient energy minimization. The 10 lowest energy structures with overall energies less than 500 kcal/mol were selected to represent the 3D folds. Structural quality was analyzed using AQUA and PROCHECK-NMR (*36*). Graphical images were prepared with MOLMOL (*37*) and PyMol version 0.99 (*38*).

RESULTS

Assignment of Resonances. The *Rb. sphaeroides* PufX was expressed as a membrane protein of 77 residues including a His_6-tag at the C-terminus. There is an uneven distribution in the amino acids as characterized by 8 Gly, 8 Leu, and 7 Ala residues. Figure 1 shows the 2D ^{1}H-^{15}N HSQC spectrum of PufX in $CDCl_3/CD_3OH$ (1:1, v/v). It exhibited a very limited chemical shift dispersion characteristic of helical proteins. Most backbone sequential assignments were made by the HNCA experiment, which correlates the C_α resonances

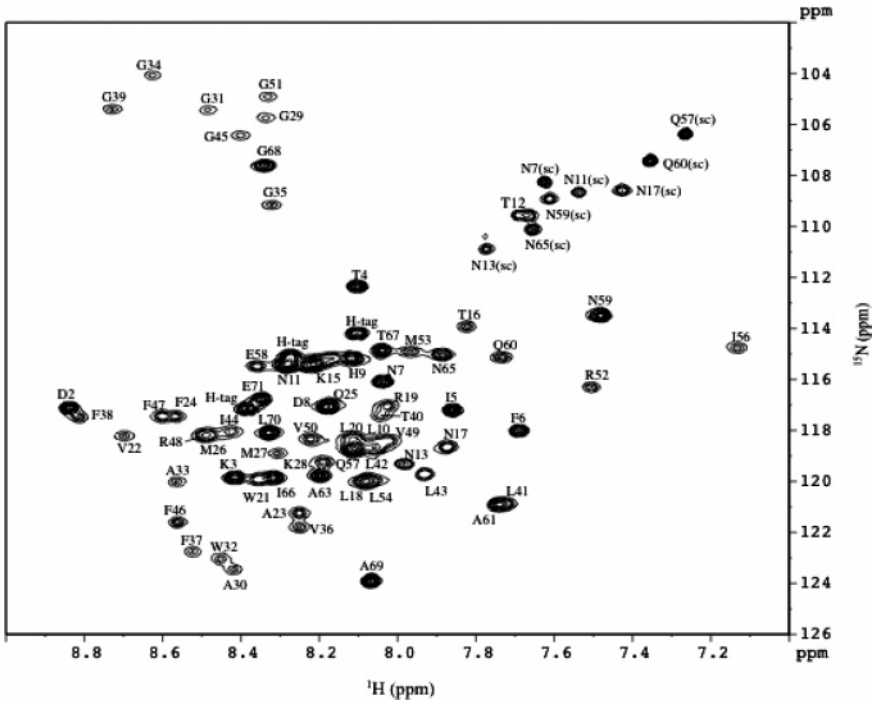

FIGURE 1: ^{1}H-^{15}N HSQC spectrum of *Rb. sphaeroides* PufX. The spectrum was recorded using 2 mM ^{15}N-labeled protein in $CDCl_3/CD_3$-OH (1:1, v/v) at 25 °C. Backbone amide cross-peaks are labeled according to residue type and sequence number. The resonances with an additional label of (sc) correspond to Gln and Asn side-chain NH_2 groups. The signals labeled with an H-tag denote the resonances from the C-terminal His-tag.

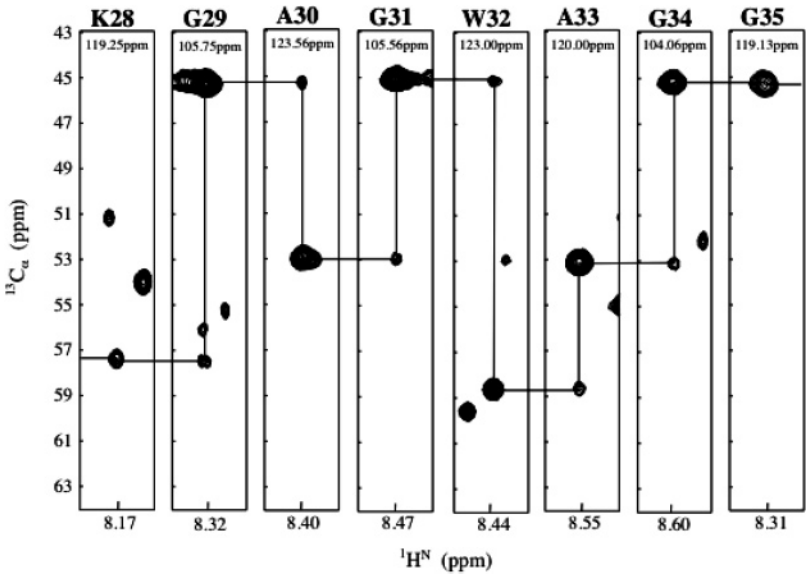

FIGURE 2: Selected 3D HNCA strips of sequential connectivities for residues Lys28−Gly35 of PufX. The ^{15}N chemical shift is shown in each panel.

of the preceding residue with intraresidue backbone ^{15}N, H^N, and C_α resonances, combined with other triple-resonance measurements using the ^{13}C- and ^{15}N-labeled samples. A typical example of the HNCA strips is shown in Figure 2 for the sequential connectivities from Lys28 to Gly35. However, because of the heavy overlap of amide resonances, backbone sequential assignment could not be completed with the sample measured in $CDCl_3/CD_3OH$. From a series of H−D exchange experiments, we noticed that most backbone amide resonances of the residues in the transmembrane domain remained observable over more than 10 days at 25 °C in the perdeuterated solvent. We decided to measure the similar 3D spectra with the PufX dissolved in $CDCl_3/CD_3$-OD (1:1, v/v). This proved to be useful, and all backbone amide and C_α resonances were assigned. The result of the assignment for the amide resonances is shown in Figure 1.

All backbone amide protons of the central hydrophobic domain had chemical shifts in a range of $\delta_H = 7.8-8.8$ ppm. The strongest signals and best resolution were observed for residues at both ends of the PufX. Resonances from side-chain NH_2 groups of Asn and Gln residues were assigned by CBCA(CO)NH measurements. The side-chain amide proton signals of Q25(sc) appeared at 6.58 and 5.57 ppm and, therefore, were not included in Figure 1. Assignments of other side-chain resonances were made by ^{15}N TOCSY-HSQC combined with 3D CBCANH, HBHANH, and H

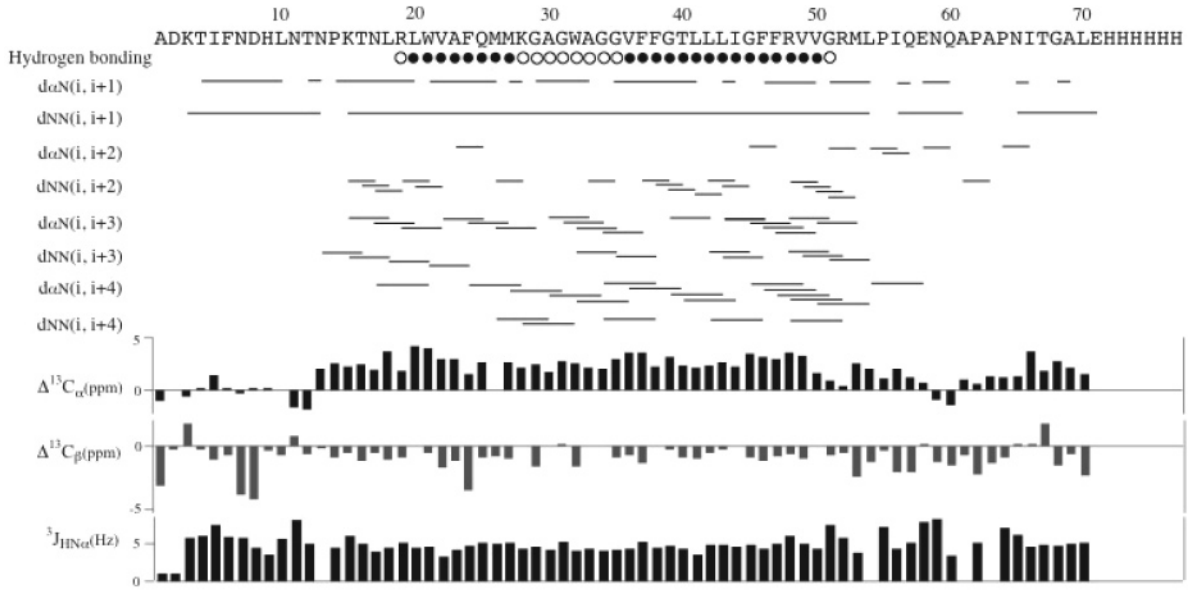

FIGURE 3: Summary of the NMR restraints used for calculating the structures of *Rb. sphaeroides* PufX. (●) Strong hydrogen bonding of the amide protons with half-lives longer than 96 h; (○) moderately strong hydrogen bonding with half-lives longer than 48 h but shorter than 96 h. Sequential NOEs are presented as continuous lines extending over the peptide segment, and inter-residue NOEs are shown by lines connecting the starting and ending residues. Secondary $^{13}C_\alpha$ and $^{13}C_\beta$ chemical shifts and $^3J(H^N, H_\alpha)$ coupling constants are shown by the histograms.

(CC)(CO)NH spectra. Assignments of the PufX protein have been deposited at the BMRB (accession number: 10024).

Structure Determinations. A total of 511 unambiguous NOE-derived distance restraints was obtained from 3D ^{15}N NOESY-HSQC experiments for the PufX protein. Figure 3 summarizes the details of the amide NOE patterns. Strong NOEs were confirmed for the $H^N(i)$ and $H^N(i + 1)$ pairs over extensive ranges of the residues, which is considered a characteristic of an α-helix. Average numbers of NOE restraints per residue were 16.1 for the residues in the central regions from Val22 to Gly51. We have identified a total of 33 consecutive hydrogen bonds for the amide protons of the PufX protein on the basis of a series of H−D exchange experiments measured in $CDCl_3/CD_3OD$ (1:1), indicating that PufX forms a stable secondary structure over its central domain. Of these, 23 backbone amide protons were evaluated as being strongly hydrogen bonded with their half-lives longer than 96 h. It was of interest to note that a short segment (Lys28−Gly35) rich in Gly and Ala residues revealed a relatively fast decay in backbone amide signals compared to the exchange time of their neighboring residues (Figure 4). This indicates that the Gly- and Ala-rich segment is more accessible to the surrounding solvent molecules and may provide crucial insight into the function of PufX as a key component of quinone exchange (see below). The hydrogen-bonding information was included as additional distance restraints in the structure calculation. Secondary $^{13}C_\alpha$ and $^{13}C_\beta$ chemical shifts were extracted and showed a characteristic of the α helix based on the empirical correlation between these values and the protein backbone conformation in terms of the ϕ and ψ torsion angles (*39*, *40*). $^3J(H^N, H_\alpha)$ coupling constants measured with HNHA experiments fell in a range of 4−6 Hz for most of the residues in the central portions and in somewhat greater values for the residues at terminal ends. All of the torsion angle information suggests that the *Rb. sphaeroides* PufX is largely α helical over the central hydrophobic region, consistent with the results from

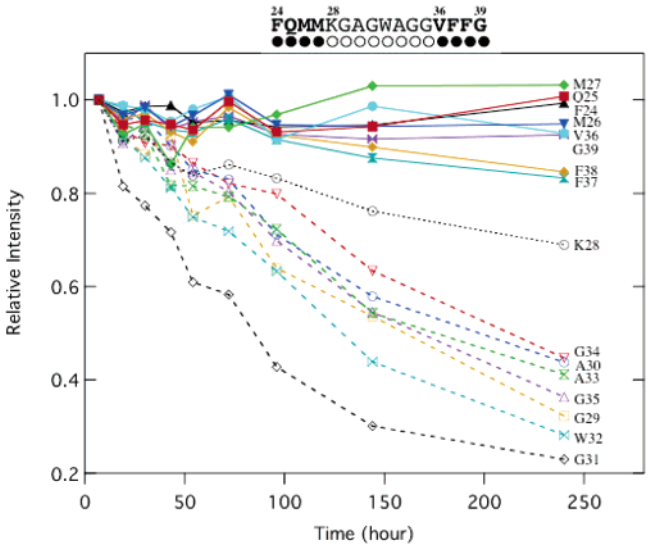

FIGURE 4: Changes of the relative intensities of the backbone amide signals from Phe24 to Gly39 in the ^1H-^{15}N HSQC spectrum as a function of time of H−D exchange. The residues marked by the open circles at the top of the Figure exhibited relatively fast decays and are plotted as dashed lines in the Figure, whereas the neighboring residues are marked by filled circles at the top of the Figure and plotted as the solid lines.

hydrogen bonding. Using the NOE derived distance constraints, the hydrogen-bonding constraints and constraints for torsion angles (ϕ and ψ) derived from the ^{13}C chemical shifts and $^3J(H^N, H_\alpha)$, the structure of PufX was calculated and energy minimized.

Description of the NMR Solution Structure. The NMR solution structures of *Rb. sphaeroides* PufX are shown in Figure 5, and quantitative evaluations of the calculated structures are summarized in Table 1. The backbone traces of the ensemble (Figure 5, left) was obtained by superimposing the backbone coordinates from Arg19 to Gly51on the 10 lowest energy structures. The structures revealed a well-

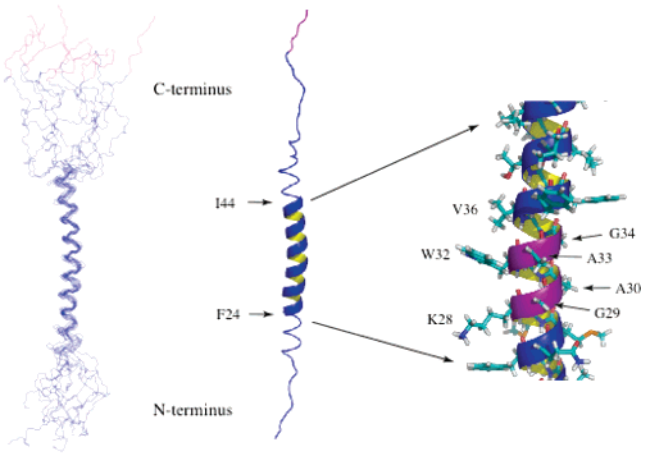

FIGURE 5: Solution structure of the *Rb. sphaeroides* PufX in $CDCl_3$/CD_3OH (1:1, v/v). Backbone traces (left side) represent the 10 lowest energy conformers obtained by superimposing the backbone atoms of residues Arg19−Gly51. Ribbon representation (middle) shows the mean structure obtained from the 10 conformers. The helical region is enlarged to show the side-chain conformation (right side), where the backbone portion of the short segment (Lys28−Gly35) is colored purple. The C-terminal His-tags are colored magenta.

Table 1: Structural Statistics for the *Rb. sphaeroides* PufX Membrane Protein

NOE distance constraints	511
intraresidue	190
sequential	200
medium-range ($i - j = 2,3,4$)	121
long-range ($i - j > 4$)	0
hydrogen bonds	33
angle constraints	165
NOE constraint violations	
largest (Å)	2.01
r.m.s. deviation (Å)	0.44
r.m.s. deviation from the mean structure (Å)	
all residues	
backbone atoms	5.92 ± 0.99
all heavy atoms	7.20 ± 1.21
residues in α-helices[a]	
backbone atoms	0.95 ± 0.30
all heavy atoms	2.00 ± 0.49
Ramachandran plots	
residues in allowed region	90.8%
residues in disallowed region	9.2%
r.m.s. deviation from ideal geometry	
bond lengths (Å)	0.0018 ± 0.0004
bond angles (deg)	0.359 ± 0.024
improper (deg)	0.184 ± 0.036

[a] The residues for calculating the rms deviations are Phe24−Ile44.

defined α helical region in the central hydrophobic domain. Backbone root-mean-square (rms) deviation over the 21 residues from Phe24 to Ile44 was 0.95 Å, and this region can be considered as a highly conserved α helix. Both N- and C-terminal domains were unstructured, and the His-tag at the C-terminus seemed not to have a significant influence on the whole structure. The ribbon representation (Figure 5, middle) shows the mean structure obtained from the 10 energy minimized structures and is characterized by an almost straight, long α helix. When the side-chains were added to the ribbon structure (Figure 5, right), it became clear that the Gly- and Ala-rich segment (Lys28−Gly35) is located in the middle of the central helix. Residues with large side chains (Lys28, Trp32, and Val36) are aligned on one side of the helix, whereas the small residues (Gly29, Ala30, Gly31, Ala33, Gly34, and Gly35) are aligned on the other face. This structural motif forms an extensive groove on the surface of the helix, which may serve as a functional site responsible for the quinone exchange and the interaction with neighboring polypeptides, for example, LH1 α- and/or β-polypeptides.

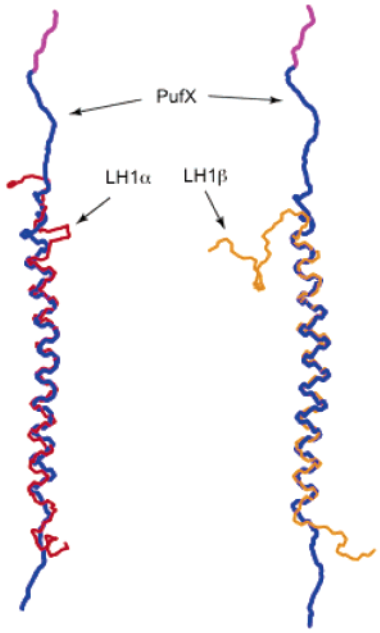

FIGURE 6: Comparison of the backbone structures of the *Rb. sphaeroides* PufX (blue) with those of the *R. rubrum* LH1 α- (red) and β (orange)-polypeptides. The C-terminal His-tags in the *Rb. sphaeroides* PufX are colored magenta.

Figure 6 shows a comparison of the backbone structures between PufX and LH1 polypeptides. The overall structure of the *Rb. sphaeroides* PufX is very similar to the solution structures of the LH1 α- and β-polypeptides from *R. rubrum*, (*20*) and the crystal structures of LH2 polypeptides from *Rps. acidophila* (*4*) and *Phaeospirillum* (*Ps.*, formerly *Rhodospirillum*) *molischianum* (*5*). The central helical domain of the PufX can be well superimposed with those of the *R. rubrum* LH1 α- and β-polypeptides over a range of about 30 residues. There is no structural information available for the *Rb. sphaeroides* LH1 α-polypeptide. Solution structures of the *Rb. sphaeroides* LH1 β-polypeptide were determined in both organic solvent and detergent solution (*41*, *42*) and showed a bent conformation with two short α-helical portions joined by a flexible central hinge. The C-terminal helix was shown to transverse the membrane, and the N-terminal helix was partially embedded in the membrane.

DISCUSSION

Circular dichroism measurements showed that the PufX expressed had an α-helix content of 29% in organic solvent (*19*), suggesting that the PufX contains a substantial α-helical region composed of about 22 amino acid residues (*19*). Similar numbers were also obtained for the native and synthesized PufX (*18*, *43*). The results are in good agreement with the structure determined in this study, which shows that the highly conserved α-helical region with the backbone rms deviation within 0.95 Å is composed of 21 residues (Phe24−Ile44). The most important feature of the PufX structure is

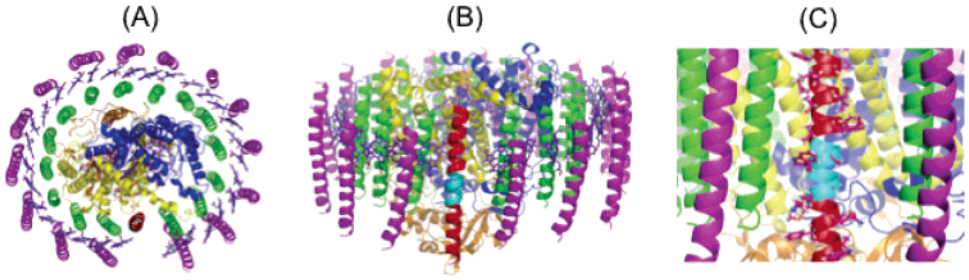

FIGURE 7: Schematic model for the LH1−RC-PufX complex. The structure was adopted from the crystal structure of LH1−RC (pdb entry: 1PYH) from *Rps. palustris*, in which helix W was replaced by the structure of the *Rb. sphaeroides* PufX determined in this study. Transmembrane helices are represented by ribbons and colored yellow for the L subunit, blue for the M subunit, orange for the H subunit, green for the LH1 α-polypeptide, purple for the LH1 *β*-polypeptide, and red for PufX. The short segment (Lys28−Gly35) in PufX is colored cyan. Macrocycles of BChl *a* are represented by sticks. (A) Top view showing the relative position of PufX in the LH1−RC-PufX complex. (B) Side view, looking from the opening of the LH1 ring. (C) Enlarged side view showing the surroundings of the Gly- and Ala-rich segment in PufX, where side chains are added to the structure of PufX. For clarity, BChl *a* macrocycles are omitted.

that a short segment rich in Gly and Ala residues (Lys28−Gly35) is located in the center of the hydrophobic membrane-spanning domain and, together with residues around this region, forms a groove-like conformation. As a result, the backbone of the segment is easily accessible to the solvents compared to its neighboring regions, as confirmed by the H−D exchange experiment. Such a conformation of the PufX might form part of a pathway for the ubiquinol movement from RC into the membrane phase and could also facilitate transmembrane helix−helix interaction. It has been known that the GxxxG motif, where two glycine residues are separated by any three amino acids on a helical framework, occurs frequently in the transmembrane domain of integral membrane proteins and acts as a universal scaffold for the transmembrane helix−helix association (*44*−*47*). This arrangement of glycine residues gives rise to a groove on one face of the helix and permits a close approach of interacting helices through van der Waals interactions. A similar GxxxA pattern is also known as an alternative of the GxxxG motif and works in a similar way for mediating the helix−helix interactions in both membrane and soluble proteins (*48*, *49*). Both structural motifs can be found in several places in the PufX sequence around the Gly- and Ala-rich segment, that is, G_{29}AGWAGGVFFG$_{39}$. Coincidentally, this sequence also matches another motif, V/IxGx$_{1-2}$GxxGxxxG, that has been proposed to form FAD and NAD(P) binding folds in oxidoreductases through C_α-H−O hydrogen bonds and van der Waals interactions (*48*).

Our proposal about the Gly and Ala-rich segment from Lys28 to Gly35 as a possible functional site of the PufX is also consistent with biochemical evidence. The *E. coli*-expressed PufX has been shown to inhibit the reconstitutions of both LH1 and B820 type complexes using α- and *β*-polypeptides and BChl *a* (*19*). Characterization of the roles of different portions of the PufX has been conducted using truncated polypeptides by synthetic and genetic methods. The results suggest that the central core region is responsible for the inhibition caused by specific interaction with LH1 α-polypeptide (*43*) and BChl *a* (*50*), whereas the N- and C-terminal domains are mainly involved in dimerization and PufX assembly (*51*), respectively. A chemically synthesized core fragment containing 25 amino acids (Gln25−Val49) of the *Rb. sphaeroides* PufX was shown to cause 50% inhibition of LH1 formation (*43*). This fragment matches well the highly conserved α-helical region (Phe24−Ile44) as determined in this study and contains the Gly- and Ala-rich segment.

The native *Rb. sphaeroides* PufX is abundant in glycine and alanine residues, accounting for 22% of total amino acids. A similar proportion of 21% is obtained for the mature *Rb. capsulatus* PufX, although the sequence homology is very low, only 23%, between the two PufX proteins. It is of interest to note that 8 of the 10 Gly residues in the *Rb. capsulatus* PufX are located in the central core region. These residues, together with Ala, form several GxxxG and GxxxA motifs in this region, which might play a role similar to that of the Gly- and Ala-rich segment in the *Rb. sphaeroides* PufX. These motifs may also contribute to a possible self-association, in a way similar to that of glycophorin A, as suggested by a recent study on the *Rb. capsulatus* PufX (*52*).

With the structure of the *Rb. sphaeroides* PufX available, we attempted to construct a structural model for the LH1−RC-PufX complex. The recent crystal structure of LH1−RC from *Rps. palustris* at 4.8 Å resolution (pdb accession code 1PYH) (*14*) was adopted as a starting model, in which the coordinates of RC from *Rb. sphaeroides* were used. From the density map of the *Rps. palustris* LH1−RC, a misoriented inner-ring helix W was found to interrupt the repeating α*β* units and could not be satisfactorily assigned to the putative 16th LH1 α-polypeptide. Because of its position close to the secondary electron acceptor ubiquinone (UQ_B) site, helix W was suggested to form part of a gate to facilitate UQ_BH_2 transport to the membrane phase and may also play a major role in the positioning of RC within the LH1−RC complex (*14*). We assumed that polypeptide W is an analogue of PufX and replaced it with the PufX in its original structure. Figure 7 illustrates such a structural model comprising LH1−RC and the PufX protein, in which the PufX is aligned to the position of polypeptide W. It has been known that the binding site of UQ_B in RC is formed exclusively by the residues of the L subunit, particularly involving transmembrane helices D and E (*53*). From Figure 7, it can be seen that PufX is located next to helix D of the L subunit (yellow) and at the center of the opening of the oval LH1 ring. Because of the close proximity, PufX could readily interact with the neighboring LH1 α-polypeptides, and a pathway might be formed between the Gly- and Ala-rich segment in the PufX and the LH1 α-polypeptide through which UQ_BH_2 is thought to move into the quinone pool. If we align the membrane-spanning regions of PufX and *Rb. sphaeroides* LH1

α-polypeptide, the Gly- and Ala-rich segment of PufX is located near the center of the transmembrane domain of the LH1 α-polypeptide. This region of the LH1 α-polypeptide contains many residues with large side chains, such as Arg, Val, Phe, and Leu, and is likely to form a ridge-like conformation to facilitate interaction with the groove-like segment of PufX. To further verify these speculations, a higher-resolution structure of a PufX-containing LH1−RC complex is needed.

ACKNOWLEDGMENT

We thank Mr. M. Kudo for his technical assistance.

REFERENCES

1. Deisenhofer, J., Epp, O., Miki, K., Huber, R., and Michel, H. (1985) Structure of the protein subunits in the photosynthetic reaction centre of *Rhodopseudomonas viridis* at 3 Å resolution, *Nature 318*, 618−624.
2. Allen, J. P., Feher, G., Yeates, T. O., Komiya, H., and Rees, D. C. (1987) Structure of the reaction center from *Rhodobacter sphaeroides* R-26: The cofactors, *Proc. Natl. Acad. Sci. U.S.A. 84*, 5730−5734.
3. Nogi, T., Fathir, I., Kobayashi, M., Nozawa, T., and Miki, K. (2000) Crystal structures of photosynthetic reaction center and high-potential iron-sulfur protein from *Thermochromatium tepidum*: Thermostability and electron transfer, *Proc. Natl. Acad. Sci. U.S.A. 97*, 13561−13566.
4. McDermott, G., Prince, D. M., Freer, A. A., Hawthornthwaite-Lawless, A. M., Papiz, M. Z., Cogdell, R. J., and Isaac, N. W. (1995) Crystal structure of an integral membrane light-harvesting complex from photosynthetic bacteria, *Nature 374*, 517−521.
5. Koepke, J., Hu, X., Muenke, C., Schulten, K., and Michel, H. (1996) The crystal structure of the light-harvesting complex II (B800-B850) from *Rhodospirillum molischianum*, *Structure 4*, 581−597.
6. Karrasch, S., Bullough, P. A., and Ghosh, R. (1995) The 8.5 Å projection map of the light-harvesting complex I from *Rhodospirillum rubrum* reveals a ring composed of 16 subunits, *EMBO J. 14*, 631−638.
7. Jamieson, S. J., Wang, P., Qian, P., Kirkland, J. Y., Conroy, M. J., Hunter, C. N., and Bullough, P. A. (2002) Projection structure of the photosynthetic reaction centre-antenna complex of *Rhodospirillum rubrum* at 8.5 Å resolution, *EMBO J. 21*, 3927−3935.
8. Fotiadis, D., Qian, P., Philippsen, A., Bullough, P. A., Engel, A., and Hunter, C. N. (2004) Structural analysis of the reaction center light-harvesting complex I photosynthetic core complex of *Rhodospirillum rubrum* using atomic force microscopy, *J. Biol. Chem. 279*, 2063−2068.
9. Scheuring, S., Seguin, J., Marco, S., Levy, D., Robert, B., and Rigaud, J.-L. (2003) Nanodissection and high-resolution imaging of the *Rhodopseudomonas viridis* photosynthetic core complex in native membranes by AFM, *Proc. Natl. Acad. Sci. U.S.A. 100*, 1690−1693.
10. Scheuring, S., Rigaud, J.-L., and Sturgis, J. N. (2004) Variable LH2 stoichiometry and core clustering in native membrane of *Rhodospirillum photometricum*, *EMBO J. 23*, 4127−4133.
11. Jungas, C., Ranck, J.-L., Rigaud, J.-L., Joliot, P., and Vermeglio, A. (1999) Supramolecular organization of the photosynthetic apparatus of *Rhodobacter sphaeroides*, *EMBO J. 18*, 534−542.
12. Scheuring, S., Francia, F., Busselez, J., Melandris, B. A., Rigaud, J.-L., and Levy, D. (2004) Structural role of PufX in the dimerization of the photosynthetic core complex of *Rhodobacter sphaeroides*, *J. Biol. Chem. 279*, 3620−3626.
13. Qian, P., Hunter, C. N., and Bullough, P. A. (2005) The 8.5 Å projection structure of the core RC-LH1-PufX dimer of *Rhodobacter sphaeroides*, *J. Mol. Biol. 349*, 948−960.
14. Roszak, A. W., Howard, T. D., Southall, J., Gardiner, A. T., Law, C. J., Isaac, N. W., and Cogdell, R. J. (2003) Crystal structure of the RC-LH1 core complex from *Rhodopseudomonas palustris*, *Science 302*, 1969−1972.
15. Farchaus, J. W., Barz, W. P., Grünberg, H., and Oesterhelt, D. (1992) Studies on the PufX polypeptide and its requirement for photoheterotrophic growth in *Rhodobacter sphaeroides*, *EMBO J. 11*, 2779−2788.
16. Barz, W. P., Francia, F., Venturoli, G., Melandri, B. A., Vermeglio, A., and Oesterhelt, D. (1995) Role of PufX protein in photosynthetic growth of *Rhodobacter sphaeroides*. 1. PufX is required for efficient light-driven electron transfer and photophosphorylation under anaerobic conditions, *Biochemistry 34*, 15235−15247.
17. Barz, W. P., Vermeglio, A., Francia, F., Venturoli, G., Melandri, B. A., and Oesterhelt, D. (1995) Role of PufX protein in photosynthetic growth of *Rhodobacter sphaeroides*. 2. PufX is required for efficient ubiquinone/ubiquinol exchange between the reaction center Q_B site and the cytochrome bc_1 complex, *Biochemistry 34*, 15248−15258.
18. Recchia, P. A., Davis, C. M., Lilburn, T. G., Beatty, J. T., Parkes-Loach, P. S., Hunter, C. N., and Loach, P. A. (1998) Isolation of the PufX protein from *Rhodobacter capsulatus* and *Rhodobacter sphaeroides*: Evidence for its interaction with the a-polypeptide of the core light-harvesting complex, *Biochemistry 37*, 11055−11063.
19. Onodera, S., Suzuki, H., Shimada, Y., Kobayashi, M., Nozawa, T., and Wang, Z.-Y. (2007) Overexpression and characterization of the *Rhodobacter sphaeroides* PufX membrane protein in *Escherichia coli*, *Photochem. Photobiol. 83*, 139−144.
20. Wang, Z.-Y., Gokan, K., Kobayashi, M., and Nozawa, T. (2005) Solution structures of the core light-harvesting α and *β* polypeptides from *Rhodospirillum rubrum*: Implications for the pigment-protein and protein-protein interactions, *J. Mol. Biol. 347*, 465−477.
21. Suzuki, H., Shimada, Y., Kobayashi, M., Kudo, M., Nozawa, T., and Wang, Z.-Y. (2005) Isotopic labeling of proteins by utilizing photosynthetic bacteria, *Anal. Biochem. 347*, 324−326.
22. Davis, A. L., Keeler, J., Laue, E. D., and Moskau, D. (1992) Experiments for recording pure-absorption heteronuclear correlation spectra using pulsed field gradients, *J. Magn. Reson. 98*, 207−216.
23. Stonehouse, J., Clowes, R. T., Shaw, G. L., Keeler, J., and Laue, E. D. (1995) Minimisation of sensitivity losses due to the use of gradient pulses in triple-resonance NMR of protein, *J. Biomol. NMR 5*, 226−232.
24. Bax, A., and Pochapsky, S. S. (1992) Optimized recording of heteronuclear multidimensional NMR spectra using pulsed field gradients, *J. Magn. Reson. 99*, 638−643.
25. Grzesiek, S., and Bax, A. (1992) An efficient experiment for sequential backbone assignment of medium-sized isotopically enriched proteins, *J. Magn. Reson. 99*, 201−207.
26. Muhandiram, D. R., and Kay, L. E. (1994) Gradient-enhanced triple-resonance three-dimensional NMR experiments with improved sensitivity, *J. Magn. Reson., Ser. B 103*, 203−216.
27. Wang, A. C., Lodi, P. J. J. Q., Vuister, G. W., Gronenborn, A. M., and Clore, G. M. (1994) An efficient triple-resonance experiment for proton-directed sequential backbone assignment of medium-sized proteins, *J. Magn. Reson., Ser. B 105*, 196−198.
28. Grzesiek, S., and Bax, A. (1993) Amino acid type determination in the sequential assignment procedure of uniformly $^{13}C/^{15}N$-enriched proteins, *J. Biomol. NMR 3*, 185−204.
29. Grzesiek, S., Anglister, J., and Bax, A. (1993) Correlation of backbone amide and aliphatic side-chain resonances in $^{13}C/^{15}N$-enriched proteins by isotropic mixing of ^{13}C magnetization, *J. Magn. Reson., Ser. B 101*, 114−119.
30. Logan, T. M., Olejniczak, E. T., Xu, R. X., and Fesik, S. W. (1993) A general method for assigning NMR spectra of denatured proteins using 3D HC(CO)NH-TOCSY triple resonance experiments, *J. Biomol. NMR 3*, 225−231.
31. Vuister, G. W., and Bax, A. (1993) Quantitative J correlation: a new approach for measuring homonuclear three-bond $J(H^NH^\alpha)$ coupling constants in ^{15}N-enriched proteins, *J. Am. Chem. Soc. 115*, 7772−7777.
32. Delaglio, F., Grzesiek, S., Zhu, G., Vuister, G. W., Pfeifer, J., and Bax, A. (1995) NMRPipe: a multidimensional spectral processing system based on UNIX pipes, *J. Biomol. NMR 6*, 277−293.
33. Johnson, B. A., and Blevins, R. A. (1994) NMRView: a computer program for the visualization and analysis of NMR data, *J. Biomol. NMR 4*, 603−614.
34. Brunger, A. T., Adams, P. D., Clore, G. M., DeLano, W. L., Gros, P., Grosse-Kunstleve, R. W., Jiang, J.-S., Kuszewski, J., Nilges, M., Pannu, N. S., Read, R. J., Rice, L. M., Simonson, T., and Warren, G. L. (1998) Crystallography & NMR system: a new software suite for macromolecular structure determination, *Acta Crystallogr., Sect. D 54*, 905−921.

35. Kuszewski, J., Qin, J., Gronenborn, A. M., and Clore, G. M. (1995) The impact of direct refinement against ^{13}Ca and ^{13}Cb chemical shifts on protein structure determination by NMR, *J. Magn. Reson., Ser. B 106*, 92−96.
36. Laskowski, R. A., Rullmann, J. A. C., MacArthur, M. W., Kaptein, R., and Thornton, J. M. (1996) AQUA and PROCHECK-NMR: Programs for checking the quality of protein structures solved by NMR, *J. Biomol. NMR 8*, 477−486.
37. Koradi, R., Billeter, M., and Wüthrich, K. (1996) MOLMOL: a program for display and analysis of macromolecular structures, *J. Mol. Graphics 14*, 51−55.
38. DeLano, W. L. (2002) DeLano Scientific, San Carlos, CA. http://pymol.sourceforge.net/.
39. Spera, S., and Bax, A. (1991) Empirical correlation between protein backbone conformation and Ca and Cb ^{13}C nuclear magnetic resonance chemical shifts, *J. Am. Chem. Soc. 113*, 5490−5492.
40. Wishart, D. S., and Sykes, B. D. (1994) The ^{13}C chemical-shift index: A simple method for the identification of protein secondary structure using ^{13}C chemical-shift data, *J. Biomol. NMR 4*, 171−180.
41. Kikuchi, J., Asakura, T., Loach, P. A., Parkes-Loach, P. S., Shimada, K., Hunter, C. N., Conroy, M. J., and Williamson, M. P. (1999) A light-harvesting antenna protein retains its folded conformation in the absence of protein-lipid and protein-pigment interactions, *Biopolymers 49*, 361−372.
42. Sorgen, P. L., Cahill, S. M., Krueger-Koplin, R. D., Krueger-Koplin, S. T., Schenck, C. C., and Girvin, M. E. (2002) Structure of the *Rhodobacter sphaeroides* light-harvesting 1 β subunit in detergent micelles, *Biochemistry 41*, 31−41.
43. Parkes-Loach, P. S., Law, C. J., Recchia, P. A., Kehoe, J., Nehrlich, S., Chen, J., and Loach, P. A. (2001) Role of the core region of the PufX protein in inhibition of reconstitution of the core light-harvesting complexes of *Rhodobacter sphaeroides* and *Rhodobacter capsulatus*, *Biochemistry 40*, 5593−5601.
44. Russ, W. P., and Engelman, D. M. (2000) The GxxxG motif: a framework for transmembrane helix-helix association, *J. Mol. Biol. 296*, 911−919.
45. Senes, A., Gerstein, M., and Engelman, D. M. (2000) Statistical analysis of amino acid patterns in transmembrane helices: the GxxxG motif occurs frequently and in association with β-branched residues at neighboring positions, *J. Mol. Biol. 296*, 921−936.
46. Kleiger, G., Grothe, R., Mallick, P., and Eisenberg, D. (2002) GXXXG and AXXXA: common α-helical interaction motifs in proteins, particularly in extremophiles, *Biochemistry 41*, 5990−5997.
47. Melnyk, R. A., Kim, S., Currant, A. R., Engelman, D. M., Bowie, J. U., and Deber, C. M. (2004) The affinity of GXXXG motifs in transmembrane helix-helix interactions is modulated by long-range communication, *J. Biol. Chem. 279*, 16591−16597.
48. Kleiger, G., and Eisenberg, D. (2002) GXXXG and GXXXA motifs stabilize FAD and NAD(P)-binding Rossmann folds through C^{α}-H·O hydrogen bonds and van der Waals interactions, *J. Mol. Biol. 323*, 69−76.
49. Kairys, V., Gilson, M. K., and Luy, B. (2004) Structural model for an AXXXG-mediated dimer of surfactant-associated protein C, *Eur. J. Biochem. 271*, 2086−2092.
50. Law, C. J., Chen, J., Parkes-Loach, P. S., and Loach, P. A. (2003) Interaction of bacteriochlorophyll with the LH1 and PufX polypeptides of photosynthetic bacteria: use of chemically synthesized analogs and covalently attached fluorescent probes, *Photosynth. Res. 75*, 193−210.
51. Francia, F., Wang, J., Zischka, H., Venturoli, G., and Oesterhelt, D. (2002) Role of the N- and C-terminal regions of the PufX protein in the structural organization of the photosynthetic core complex of *Rhodobacter sphaeroides*, *Eur. J. Biochem. 269*, 1877−1885.
52. Aklujkar, M., and Beatty, J. T. (2006) Investigation of *Rhodobacter capsulatus* PufX interactions in the core complex of the photosynthetic apparatus, *Photosynth. Res. 88*, 159−171.
53. Okamura, M. Y., and Feher, G. (1995) Proton-Coupled Electron Transfer Reactions of Q_B in Reaction Centers from Photosynthetic Bacteria, in *Anoxygenic Photosynthetic Bacteria* (Blankenship, R. E., Madigan, M. T., and Bauer, C. D., Eds.) pp 577−594, Kluwer Academic Publishers, Dordrecht, The Netherlands.

BI0618060